CHEMISTRY OF MATERIALS
Article

Chem. Mater. **2010,** *22,* 5453–5462 5453
DOI:10.1021/cm100816h

^{2}H and ^{7}Li Solid-State MAS NMR Study of Local Environments and Lithium Adsorption on the Iron(III) Oxyhydroxide, Akaganeite (β-FeOOH)

Jongsik Kim[†] and Clare P. Grey*[,†,‡]

[†]*Department of Chemistry, Stony Brook University, New York 11794-3400, and* [‡]*Department of Chemistry, Cambridge University, Lensfield Road, Cambridge, United Kingdom CB2 1EW*

Received March 22, 2010. Revised Manuscript Received August 19, 2010

^{2}H and ^{7}Li MAS NMR spectroscopy have been applied to characterize the surface and bulk hydroxyl groups and Li^{+} sorption on the iron oxyhydroxide akaganeite (β-FeOOH), a common soil mineral with a large surface area and uptake capacity for toxic cations and anions. The formation of both inner and outer-sphere complexes on the surface of akaganeite was confirmed, the former giving rise to ^{7}Li NMR signals with large ^{7}Li hyperfine shifts. The concentrations of these complexes was determined as a function of pH and possible Li^{+} binding modes and sites are proposed based on their ^{7}Li hyperfine shifts. The binding is compared with those of the other FeOOH polymorphs, goethite and lepidocrocite. The modes of binding are similar to those of goethite, except that sites at the entrances to the tunnels become available for binding, particularly for nanosized akaganeite particles.

1. Introduction

Iron oxyhydroxides (FeOOH), such as α-, β-, and γ-types, have distinctive properties as pigments,[1] catalysts,[1,2] semiconductors,[3,4] and electrode materials,[2,5,6] and are precursors for magnetic recording media materials such as Fe_3O_4 and γ-Fe_2O_3.[1,7,8] Moreover, they are attractive adsorbents for removing toxic ions such as Pb^{2+}, Cd^{2+}, Cr^{6+}, and $As^{3+/5+}$ from polluted water and nuclear waste streams, because of their high adsorption capacities and availability and low cost.[1,9−16] Thus, it is important to understanding the interactions between these iron oxyhydroxides and metal ions in order to both predict the destiny of the adsorbed metal ions in groundwater and to design more effective systems to remove the toxic metals. In addition, the development of methods to detect and determine the modes of adsorption of cations such a Li^{+}, Na^{+}, and Ag^{+} can also help in the design of sensors for these ions.[17,18]

Many studies have been performed to determine the adsorption modes (for molecules and ions) and the binding sites on iron-containing minerals, by means of spectroscopic methods such as IR and X-ray absorption spectroscopy (XAS).[10,19−27] However, the binding mechanisms are generally far from clear, and often controversial. This is especially true for small cations such as Li^{+}, Na^{+}, and Mg^{2+}, where XAS methods cannot be applied. For these light cations, solid-state NMR spectroscopy is a

*To whom correspondence should be addressed. E-mail: cgrey@notes.cc.sunysb.edu.

(1) Cornell, R. M.; Schwertmann, U. *The Iron Oxides*; VCH: New York, 1996.
(2) Huber, D. L. *Small* **2005**, *1*, 482.
(3) Leland, J. K.; Bard, A. J. *J. Phys. Chem.* **1987**, *91*, 5076.
(4) White, A. F. In *Interface Geochemistry*; Reviews in Mineralogy; Mineral Society of America: Washington, D.C., 1990; Vol. *23*.
(5) Amine, K.; Yasuda, H.; Yamachi, M. *J. Power Sources* **1999**, *81−82*, 221.
(6) Matsumura, T.; Kanno, R.; Inaba, Y.; Kawamoto, Y.; Takano, M. *J. Electrochem. Soc.* **2002**, *149*, A1509.
(7) Moon, J. W.; Roh, Y.; Lauf, R. J.; Vali, H.; Yeary, L. W.; Phelps, T. J. *J. Microbiol. Methods* **2007**, *70*, 150.
(8) Zhang, L.-Y.; Xue, D.-S.; Fen, J. *J. Magn. Magn. Mater* **2006**, *305*, 228.
(9) Deliyanni, E. A.; Bakoyannakis, D. N.; Zouboulis, A. I.; Matis, K. A. *Chemosphere* **2003**, *50*, 155.
(10) Deliyanni, E. A.; Matis, K. A. *Sep. Purif. Technol.* **2005**, *45*, 96.
(11) Chitrakar, R.; Tezuka, S.; Sonoda, A.; Sakane, K.; Ooi, K.; Hirotsu, T. *J. Colloid Interface Sci.* **2006**, *298*, 602.
(12) Lazaridis, N. K.; Bakoyannakis, D. N.; Deliyanni, E. A. *Chemosphere* **2005**, *58*, 65.
(13) Deliyanni, E. A.; Peleka, E. N.; Matis, K. A. *J. Hazard. Mater.* **2007**, *141*, 176.
(14) Ebner, A. D.; Ritter, J. A.; Navratil, J. D. *Ind. Eng. Chem. Res.* **2001**, *40*, 1615.
(15) Marmier, N.; Delisee, A.; Fromage, F. *J. Colloid Interface Sci.* **1999**, *211*, 54.
(16) Yavuz, C. T.; Mayo, J. T.; Yu, W. W.; Prakash, A.; Falkner, J. C.; Yean, S.; Cong, L.; Shipley, H. J.; Kan, A.; Tomson, M.; Natelson, D.; Colvin, V. L. *Science* **2006**, *314*, 964.
(17) Kanoh, H.; Feng, Q.; Miyai, Y.; Ooi, K. *J. Electrochem. Soc.* **1993**, *140*, 3162.
(18) Poul, N. L.; Baudrin, E.; Morcrette, M.; Gwizdala, S.; Masquelier, C.; Tarascon, J.-M. *Solid State Ionics* **2003**, *159*, 149.
(19) Farquhar, M. L.; Charnock, J. M.; Livens, F. R.; Vaughan, D. J. *Environ. Sci. Technol.* **2002**, *36*, 1757.
(20) Hsia, T. H.; Lo, S. L.; Lin, C. F.; Lee, D. Y. *Chemosphere* **1993**, *26*, 1897.
(21) Leuz, A. K.; Monch, H.; Johnson, C. A. *Environ. Sci. Technol.* **2006**, *40*, 7277.
(22) Mallikarjuna, N. N.; Venkataraman, A. *Talanta* **2003**, *60*, 139.
(23) Manceau, A.; Nagy, K. L.; Spadini, L.; Ragnarsdottir, K. V. *J. Colloid Interface Sci.* **2000**, *228*, 306.
(24) Peacock, C. L.; Sherman, D. M. *Geochim. Cosmochim. Acta* **2004**, *68*, 2623.
(25) Peak, D.; Sparks, D. L. *Environ. Sci. Technol.* **2002**, *36*, 1460.
(26) Randall, S. R.; Sherman, D. M.; Ragnarsdottir, K. V. *Geochim. Cosmochim. Acta* **2001**, *65*, 1015.
(27) Gossuin, Y.; Colet, J.-M.; Roch, A.; Muller, R. N.; Gillis, P. *J. Magn. Reson.* **2002**, *157*, 132.

Published on Web 09/03/2010

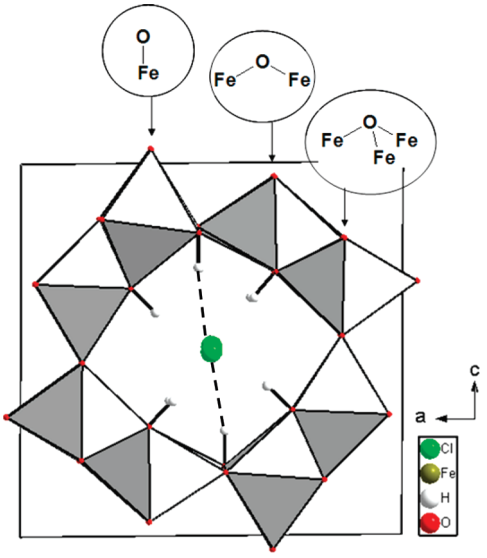

Figure 1. Crystal structure of akaganeite (β-FeOOH).[34] The FeO(H) H^+ ions are on split positions. The extra protons (required to charge balance the Cl^- tunnel ions) are those proposed in Kubicki's model (see text). The H-bonds between these ions and the Cl^- ions are shown with dashed lines.[34,39] The surface oxygen groups $Fe_3O(H)$, $Fe_2O(H)$, and $FeO(H)/FeO(H_2)$, where $Fe_xO(H_y)$ indicates that the surface oxygen ion is bound to x Fe^{3+} ions and y H^+ ions, are shown without the surface protons, because the actual number of protons attached to surface oxygen atom (y) is highly pH-dependent.

unique tool because it can detect the adsorbed species themselves. However, to date, there have been only very few solid-state NMR studies of these paramagnetic iron oxyhydroxides, the challenging magnetic properties of these systems causing rapid relaxation of the nuclear spins and large shifts and broadening of the NMR signals.[28−30]

We recently reported ^2H and $^{6,7}Li$ MAS NMR studies of Li^+ adsorption on goethite (α-FeOOH) and lepidocrocite (γ-FeOOH).[28−30] As an extension to these studies, we now report the results of Li^+ adsorption on the third FeOOH polymorph akaganeite (β-FeOOH). Akaganeite can be synthesized with large surface areas of 30−280 m^2g^{-1}, and it has a tunnel structure that may result in sorption modes that are quite different from those of the other two polymorphs.[31−33] Goethite has a Néel temperature, T_N, of above 120 °C when its particles are micrometer-sized, and it is therefore antiferromagnetically ordered at room temperature.[1] Therefore, to obtain high-resolution ^2H MAS NMR spectra at room temperature, we lowered T_N either by cation-doping or by synthesizing nanoparticles.[28] Akaganeite has a lower T_N of about 17 °C and yet it has very similar surface oxygen sites, i.e., $Fe_3O(H)$, $Fe_2O(H)$, and $FeO(H)/FeO(H_2)$ groups (Figure 1), (where the actual number of hydrogen atoms attached to each surface oxygen group (in parentheses) is highly pH-dependent). Thus, we can avoid the NMR issues related to the antiferromagnetic ordering of spins found with goethite, allowing Li^+ adsorption on akaganeite to be studied under experimental conditions that are much closer to those found in real environmental conditions.

Akaganeite, β-FeOOH, (chemical formula $FeO_{0.833}(OH)_{1.167}Cl_{0.167}$[34]) is mainly found in chloride-containing environments such as hot brines and in the corrosion of iron.[1,35,36] It is isostructural with hollandite (Figure 1),[1] the structure consisting of double chains of edge-shared Fe-octahedra, running parallel to the pseudo 4-fold symmetrical b-axis of the monoclinic unit cell (space group $I2/m$).[34,35] The double FeO_6 chains share corners with adjacent chains, forming a 2×2 tunnel structure with a cross section of 0.5 nm^2.[1] (Note that the monoclinic distortion is extremely small and is difficult to see by powder X-ray diffraction; thus the reflections are generally indexed based on the tetragonal space group ($I4/m$), the tunnels now running along the c-direction.)[37] The (100) and (001) faces, indexed in the monoclinic space group, represent the main surface planes.[1] The structure is stabilized by Cl^- ions, which are charge-balanced by additional protons in the tunnels.[38] Different models for the extra proton sites have been proposed by Post et al.[35] and Stahl et al.[34] based on neutron powder diffraction refinements. Post's model suggests that the extra protons are sufficiently close to the Fe_3OH groups, so that they can form hydrogen bonds to both the chloride ions and the oxide ions of the Fe_3OH groups, forming $Fe_3O(H)\cdots H\cdots Cl$ linkages.[35] Alternatively, Stahl's model proposes that the extra protons are placed in the corners of the tunnels, forming a hydrogen bond to the bare oxygen atoms in the corners of the tunnels, i.e., $Fe_3O\cdots H$.[34] Figure 1 shows an energetically minimized structure by Kubicki et al., where the coordinates used in Stahl's model were used as starting inputs.[39] The energetically minimized structure was obtained by projector-augmented plane wave density functional theory calculations, in combination with the Perdew−Burke−Ernzerhof pseudopotentials.[40−42] Kubicki's model similarly finds extra protons in the corners inside the tunnel structure in support of Stahl's model. However, Kubicki's model deviates from that of Stahl in that it contains a hydrogen bond between the extra proton and the Cl^- ion and in this sense, it is similar to Post's model.

The Cl^- ions ideally occupy two-thirds of the tunnel sites, but can be exchanged with other anions such as

(28) Cole, K. E.; Paik, Y.; Reeder, R. J.; Schoonen, M.; Grey, C. P. *J. Phys. Chem. B* **2004**, *108*, 6938.
(29) Nielsen, U. G.; Paik, Y.; Julmis, K.; Schoonen, M. A. A.; Reeder, R. J.; Grey, C. P. *J. Phys. Chem. B* **2005**, *109*, 18310.
(30) Kim, J.; Nielsen, U. G.; Grey, C. P. *J. Am. Chem. Soc.* **2008**, *130*, 1285.
(31) Schwertmann, U.; Cornell, R. M. *Iron Oxides in the Laboratory*; VCH: New York, 1991.
(32) Mazeina, L.; Deore, S.; Navrotsky, A. *Chem. Mater.* **2006**, *18*, 1830.
(33) Music, S.; Saric, A.; Popovic, S. *J. Mol. Struct.* **1997**, *410−411*, 153.
(34) Stahl, K.; Nielsen, K.; Jiang, J.; Lebech, B.; Hanson, J. C.; Norby, P.; van Lanschot, J. *Corros. Sci.* **2003**, *45*, 2563.
(35) Post, J. E.; Heaney, P. J.; Dreele, R. B. V.; Hanson, J. C. *Am. Mineral.* **2003**, *88*, 782.
(36) Cai, J.; Liu, J.; Gao, Z.; Navrotsky, A.; Suib, S. L. *Chem. Mater.* **2001**, *13*, 4595.
(37) Wang, X.; Chen, X.; Gao, L.; Zheng, H.; Ji, M.; Tang, C.; Shen, T.; Zhang, Z. *J. Mater. Chem.* **2004**, *14*, 905.
(38) Post, J. E.; Buchwald, V. F. *Am. Mineral.* **1991**, *76*, 272.
(39) Kubicki, J. Personal communication.
(40) Blöchl, P. E. *Phys. Rev. B* **1994**, *50*, 17953.
(41) Kresse, G.; Joubert, D. *Phys. Rev. B* **1999**, *59*, 1758.
(42) Perdew, J. P.; Burke, K.; Ernzerhof, M. *Phys. Rev. Lett.* **1996**, *77*, 3865.

OH^- and F^-, and can be partially released by washing with H_2O at neutral pH.[1,34−36,43] The existence of H_2O molecules in the tunnel sites not occupied by Cl anions is still under debate.[35,44] The protons inside the tunnel can be ion-exchanged by Li^+ ions, and by analogy with lithiated α-MnO_2, the Li^+ ions are thought to occupy vacant tetrahedral sites in the tunnels (Figure 10),[6,45] the Cl^- positions in the tunnel of akaganeite being filled with OH^- or O^{2-}.[6] The Li^+ ions are therefore coordinated to the oxygen of the OH^- or O^{2-} groups in the center of the tunnel and to the oxygen ions of the framework structure.[6]

In this study, ^2H and ^7Li MAS NMR spectroscopy was used to probe the local bulk and surface environments of deuterated and Li^+-sorbed akaganeites (β-FeOOH), as a function of pH. The results are compared with ^7Li NMR spectra of a tunnel-structured $LiFeO_2$,[6] to establish correlations between Li hyperfine shifts and local environments. The Li^+ binding sites on the surface of akaganeite are then compared with those previously reported for goethite and lepidocrocite.[29,30] Li^+ was chosen as a model ion with which to study this sorption, because we and others have reported the [6,7]Li MAS NMR spectra of various lithium-containing paramagnetic materials.[29,30,46−52] ^7Li NMR spectroscopy also represents a reasonable method for identifying and quantifying the strongest sorption sites that are likely to bind small and/or ionic cations such as Na^+ and Mg^{2+}.

2. Experimental Section

2.1. Sample Preparation. *2.1.1. Akaganeite: Micrometer-Sized Akaganeite (Aka-m).* $FeCl_3$ (8.1 g, Alfa Aesar) was dissolved in 150 mL of distilled water, and 9.0 g of urea (Aldrich) was added. The pH was adjusted to 1.5 with a 1 M NH_3 solution. The solution was refluxed for 6 h and then cooled to room temperature. The akaganeite was separated by centrifugation, washed with water several times, and dried at 60 °C.[36,53]

2.1.2. Nanosized Akaganeite (Aka-n). $FeCl_3 \cdot 6H_2O$ (2.7 g) was hydrolyzed with 1.4 g of urotropin (Aldrich) at 90 °C for 5 h in 100 mL of distilled water. The pH of the solution was 3.4. The solid product was separated from the mother liquor by centrifugation, washed with water several times, and then freeze-dried.[32,33]

2.1.3. Deuterated Akaganeite. As-synthesized akaganeite (Aka-m or Aka-n) was suspended for 1 week in D_2O (98%, Cambridge Isotope Laboratories); the suspension (which had a pH of approximately 2.0) was shaken regularly during this period, and was then centrifuged and vacuum-dried.[54]

2.1.4. Li^+ Adsorbed Akaganeite. Akaganeite (0.3 g, Aka-m) was suspended in 100 mL of distilled water. One-hundred milliliters of of a 50 mM $^7LiOH \cdot H_2O$ solution was added to the suspension. The pH was then controlled by adding appropriate quantities of either a 1 M HCl or 1 M NaOH solution to prepare three different samples at pH 3.6 (Aka-m-3.6), 7.8 (Aka-m-7.8), and 11.9 (Aka-m-11.9), where the pH was measured by a OAKTON pH 2100 series with a OAKTON glass electrode. Li sorption on the nanosized samples was also performed with Aka-n by using the same experimental procedure at pH 8.2 (Aka-n-8.2) and at pH 11.3 (Aka-n-11.3). The pH values were chosen on the basis of the measured point of zero charge (PZC), pH 7.4, for Aka-m. The solutions were stirred for a day and the Li-sorbed samples were then separated by centrifugation (5000 rpm) and dried at 80 °C in air. These experiments were repeated three times to ensure reproducibility; NMR spectra (as described below) were obtained for all the materials and no significant differences were noted between the spectra of the samples prepared under the same pH conditions.

2.1.5. Tunnel-Structured $LiFeO_2$. As-synthesized akaganeite (0.25 g, Aka-m) was added to a solution of 50 mL of ethyl ether phenyl (Aldrich) and lithium hydroxide (monohydrate) ($^7LiOH \cdot H_2O$, Aldrich) with a Li/Fe = 5 molar ratio. The solution was stirred with a magnetic stir bar and heated to 110 °C for 10 h, as described previously.[6] The reaction product was centrifuged and washed with ethanol several times and then vacuum-dried at room temperature for 1 week.

2.2. Characterization. *2.2.1. X-ray Diffraction (XRD) and Scanning Electron Microscopy (SEM) Transmission Electron Microscope (TEM).* XRD data were collected for all samples on a Rigaku Miniflex XRD benchtop X-ray diffractometer (Cr Kα radiation). The measured 2θ values were converted to those corresponding to Cu Kα radiation. All the diffraction patterns were compared with those in the Joint Committee on Powder Diffraction Standards (JCPDS). SEM images were obtained on a Leo 1550. TEM images were taken on a FEI BioTwinG^2 transmission electron microscope.

2.2.2. PZC (Point of Zero Charge), BET (Brunauer, Emmett, and Teller) Surface Area, and Elemental Analysis. Point of zero charge (PZC) was measured with a ZetaPlus (Brookhaven Instruments Corporation). No attempt was made to remove the dissolved CO_2 from the solution. The BET surface areas for akaganeite samples (Aka-m and Aka-n) were obtained on a Micromeritics ASAP 2010 gas sorption analyzer using N_2. Chloride contents of akaganeite (Aka-m and Aka-m-11.9) were analyzed commercially with a MCC-TOX-100 analyzer (Galbraith Laboratories).

2.2.3. Thermogravimetric Analysis (TGA). TGA experiments were carried out on a Netzsch (Germany), STA (simultaneous thermal analysis) 449 Jupiter instrument with a temperature ramp of 10 °C/min from ambient to 1050 °C under nitrogen as a carrier gas. Samples were dried at 80 °C under vacuum for 12 h before TGA measurements.

2.2.4. MAS (Magic Angle Spinning) NMR. ^2H MAS NMR experiments were performed at a Larmor frequency of 55.27 MHz on an INFINITY-360 spectrometer equipped with a Chemagnetics 4 mm HX MAS probe, with a rotor-synchronized, spin−echo pulse sequence and a pulse delay of 0.15 s. The ^2H NMR spectra were referenced to D_2O at 4.8 ppm. Isotropic

(43) Paterson, R.; Rahman, H. *J. Colloid Interface Sci.* **1983**, *94*, 60.
(44) Samsonov, G. *The Oxide Handbook*; IFI/Plenum: New York, 1973.
(45) Johnson, C. S.; Dees, D. W.; Mansuetto, M. F.; Thackeray, M. M.; Vissers, D. R.; Argyriou, D.; Loong, C.-K.; Christensen, L. *J. Power Sources* **1997**, *68*, 570.
(46) Levasseur, S.; Menetrier, M.; Delmas, C. *J. Power Sources* **2002**, *112*, 419.
(47) Grey, C. P.; Dupre, N. *Chem. Rev.* **2004**, *104*, 4493.
(48) Cahill, L. S.; Kirby, C. W.; Goward, G. R. *J. Phys. Chem. C* **2008**, *112*, 2215.
(49) Davis, L. J. M.; Heinmaa, I.; Goward, G. R. *Chem. Mater.* **2010**, *22*, 769.
(50) Lee, H.; Polenova, T.; Beer, R. H.; McDermott, A. E. *J. Am. Chem. Soc.* **1999**, *121*, 6884.
(51) Makimura, Y.; Cahill, L. S.; Iriyama, Y.; Goward, G. R.; Nazar, L. F. *Chem. Mater.* **2008**, *20*, 4240.
(52) Gee, B.; Horne, C. R.; Cairns, E. J.; Reimer, J. A. *J. Phys. Chem. B* **1998**, *102*, 10142.
(53) Ishikawa, T.; Nitta, S.; Kondo, S. *J. Chem. Soc., Faraday Trans. 1* **1986**, *82*, 2401.
(54) Weckler, B.; Lutz, H. D. *Eur. J. Solid State Inorg. Chem.* **1998**, *35*, 531.

resonances were identified by performing additional experiments at a different spinning speed of 13 kHz. Variable temperature experiments were performed by heating the sample to the desired temperature and waiting for an hour before starting the data acquisition. The variable-temperature experiment typically takes 3 h at high temperatures and 6 h at low temperatures, respectively, to acquire.

^{7}Li solid-state NMR spectroscopy was performed at a Larmor frequency of 77.76 MHz on a CMX-200 spectrometer equipped with a Samoson 1.8 mm MAS probe (spinning speeds of 34 - 37 kHz) and a Samoson 1.3 mm MAS probe at a spinning speed of 58 kHz. A rotor-synchronized, spin−echo pulse sequence was employed with an evolution period of one rotor period. The ^{7}Li NMR spectra were referenced to a 1.0 M ^{7}LiCl solution at 0 ppm. Spin−lattice relaxation (T_1) times were measured by using an inversion−recovery pulse sequence. Li concentrations were determined by comparing the absolute intensity of the signals (isotropic peaks and their respective spinning sidebands) obtained with a spin−echo sequence from the Li^+-sorbed akaganeite samples with that from solid Li_2CO_3. Only the hyperfine-shifted resonances and their spinning side bands (data obtained at 37 kHz) were considered. For solid Li_2CO_3, a pulse delay of 1500 s was used to acquire four scans, whereas for the Li^+-sorbed akaganeite, a pulse delay of 0.15 and 70 000 scans was used. (The pulse delay was chosen so as to be longer than $5T_1$ times ($T_1 \approx 6$ ms)). The intensities were normalized by the sample masses and the number of scans. In order to correct the intensities for signal loss during the spin−echo pulse sequence, the transverse relaxation (T_2) time was obtained by acquiring six spectra with different evolution/refocusing times and fitting the intensities obtained as a function of time to an exponential decay.

The ^{6}Li MAS NMR spectrum was acquired at a Larmor frequency of 29.45 MHz on a CMX-200 spectrometer equipped with a Samoson 1.8 mm MAS probe with a rotor-synchronized, spin−echo pulse sequence, an evolution period of one rotor period and a pulse delay of 0.2 s. The spectra were referenced to a 1.0 M ^{6}LiCl solution at 0 ppm.

3. Results and Discussion

3.1. XRD, SEM, TEM, PZC, BET Surface Area, Elemental Analysis, and TGA. The XRD powder patterns of the as-synthesized akaganeites, β-FeOOH (Aka-m and Aka-n) were unambiguously indexed on the basis of JCPDS file #34−1266 (Figure 2a, d). No significant structural modification was observed by XRD during deuteration (Figure 2b, e). The XRD patterns for the ^{7}Li-sorbed micrometer-sized akaganeites at pH 3.6, 7.8, and 11.9 are also identical to that of pristine Aka-m, indicating that lithium adsorption did not cause any noticeable long-range structural changes of the akaganeite (see the Supporting Information, Figure S1). The XRD patterns of the ^{7}Li-sorbed nanosized akaganeites are indistinguishable from those of Aka-n (not shown here). By contrast, noticeable broadening of the XRD pattern was observed after the ion exchange reaction to form tunnel-structured $LiFeO_2$. Very small shifts were seen for the hkl reflections with $l \neq 0$. No significant shifts were, however, seen for the other reflections, consistent with previous reports (Figure 2c).[6] The shifts of the $l \neq 0$ reflections can be seen most clearly for the 002 reflection (indexed in the $I4/m$ space group) near 61° 2θ, indicating a slight shrinkage along the tunnel direction, due to the ion exchange of

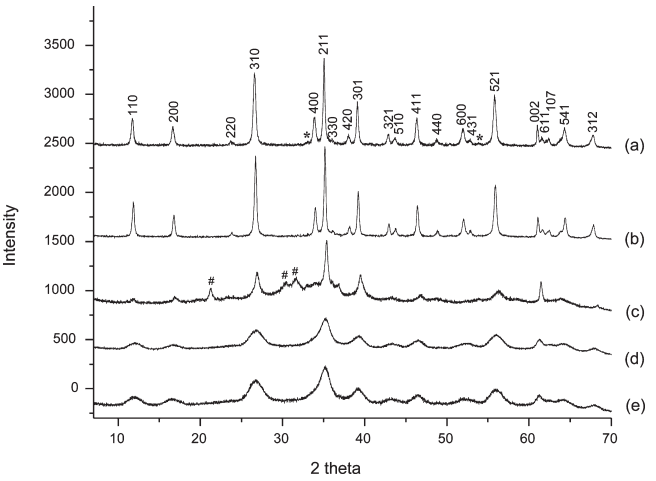

Figure 2. X-ray powder diffraction of (a) microsized FeOOH (Aka-m), (b) FeOOD (from Aka-m), (c) tunnel-structured $LiFeO_2$ (from Aka-m), (d) nanosized FeOOH (Aka-n), and (e) FeOOD (from Aka-n). * denotes the salt impurities, which were removed after deuteration and rewashing. # denotes the Li_2CO_3 impurity. The XRD reflections have been indexed with a tetragonal space group ($I4/m$), with $a = b \approx 10.53$ Å and $c \approx 3.013$ Å.[37]

H^+ with Li^+.[6] The 002 reflection is still sharp, suggesting that the coherence length along the tunnels is still large (decreasing from 314 nm for Aka-m to 52 nm, based on the Debye Scherer formula). In contrast, the coherence lengths based on the 200 and 211 reflections are only 14 and 16 nm, respectively, for the ion-exchanged material. This indicates that disorder in, for example, the Li positions, and some partial dissolution of the particles, must reduce the coherence lengths perpendicular to the tunnel directions.

In principle, the morphology adopted by akaganeite can be varied from cigar-shaped (also called somatoid in some reports)[1,55] to rodlike crystals by altering the acidity and temperature of synthetic conditions.[31,56] On the basis of the SEM (Figure 3a), our as-synthesized akaganeite (Aka-m) is rodlike, and is approximately 400 nm in length and 10 nm in width, which is a typical akaganeite morphology.[36] A TEM image of Aka-n contains 10−20 nm long and 4 nm wide rods, which is again consistent with the previously reported data for small (Aka-n) particles (Figure 3b).[32]

A PZC of pH 7.4 (±0.3) for β−FeOOH (Aka-m) was measured, consistent with the reported PZC value of pH 7.3 (see Figure S2 in the Supporting Information).[9,13,57] The measured BET surface areas for Aka-m and Aka-n were 33 and 180 m^2/g, respectively, which are consistent with values for materials synthesized by using similar methods.[31,32,36,53] TGA measurements, described more fully in the Supporting Information (Figure S3), showed that the materials are stable up to 150 °C; loss of structural water from the tunnels occurs above this temperature. During the structural transformation, about 19% weight loss was observed for Aka-m, consistent with earlier reports (see Figure S3a in the Supporting Information).[58]

(55) Gallagher, K. J. *Nature* **1970**, *226*, 1225.
(56) Richmond, W. R.; Cowley, J. M.; Parkinson, G. M.; Saunders, M. *CrystEngComm* **2006**, *8*, 36.
(57) Kanungo, S. B. *J. Colloid Interface Sci.* **1994**, *162*, 86.

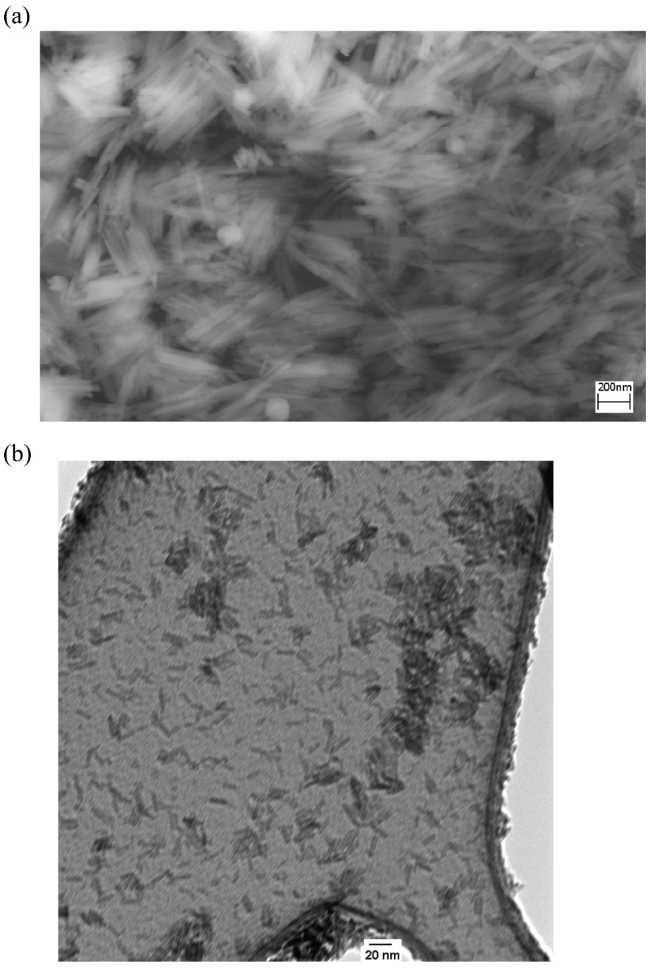

Figure 3. (a) SEM image of micrometer (β-FeOOH, Aka-m) and (b) TEM image of nano (β-FeOOH, Aka-n) akaganeite.

The total loss of water is about 22%. Aka-m-11.9 showed about 34% weight loss from room temperature to 660 °C (see Figure S3b in the Supporting Information). Aka-m and Aka-m-11.9 contain 0.78 and 0.11 wt % of Cl^-, respectively, based on the elemental analyses. Using these values, in combination with the TGA results, molecular formulas for Aka-m and Aka-m-11.9 of $FeOOH \cdot 0.022Cl \cdot 0.79H_2O$ and $FeOOH \cdot 0.003Cl \cdot 1.8H_2O$, respectively, were estimated where the water content given here includes the surface water. (If we assume all the surface water has been removed by 150 °C, a formula for Aka-m of $FeOOH \cdot 0.022Cl \cdot 0.58H_2O$ is obtained, the $0.58H_2O$ per formula unit representing the tightly bound water in the tunnels and on the surfaces.) From this data, it is obvious that the Cl^- content of our materials is low and that it is further reduced during the Li^+ sorption reactions performed at pH 11.9.[36] Nanosized akaganeite (Aka-n) showed 19.8% weight loss from room temperature to 850 °C (see Figure S3c in the Supporting Information).

3.2. Solid-State NMR. *3.2.1. ^2H NMR of β-FeOOD (Aka-m and Aka-n).* The envelope of the ^2H MAS NMR spectrum of β-FeOOD (Aka-m and Aka-n) corresponds to a typical Pake-doublet, indicating that there are rigidly

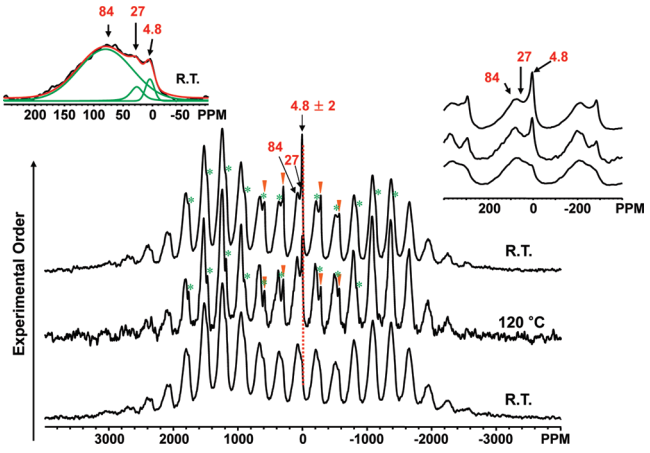

Figure 4. Variable-temperature ^2H MAS NMR spectra of β-FeOOH (Aka-m) at RT, 120 °C, and then upon returning to RT (from bottom to top). The isotropic resonances are labeled with their hyperfine shifts in this and in subsequent plots. (Spinning speed = 16 kHz). Left upper corner inset: Deconvolution of the spectrum acquired at room temperature before heating the sample (green peaks and red lines (sum)). The sidebands of the 4.8 and 27 ppm resonances are marked with orange triangles and green asterisks, respectively.

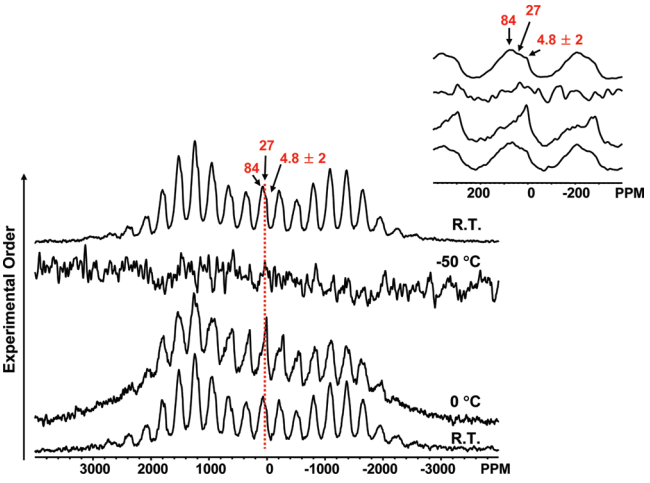

Figure 5. Variable-temperature ^2H MAS NMR spectra of β-FeOOH (Aka-m) at RT, −50 °C, and then upon returning to RT (spinning speed = 16 kHz).

bound hydroxyl groups in the structure. (Figures 4−6). The slight asymmetry of the envelope of the spectra is attributed to the anisotropic, dipolar interactions between the ^2H nuclei and unpaired electron spins of Fe^{3+} (d^5, high spin).[50] Two local environments were observed in the spectrum of Aka-m with isotropic resonances at 27 and 84 ppm (Figures 4 and 5) and signal intensities of approximately 1:10, respectively, although the significant overlap between the resonances introduces uncertainties in the determination of relative intensities. (Note that although weak, the 27 ppm resonance is clearly seen as a shoulder on all the sidebands of the 84 ppm resonance throughout the whole sideband manifold.) A third, very weak resonance is observed at 4.8 ppm, which is assigned to surface water. This resonance is presumably weak because the samples were vacuum-dried overnight, to remove all the weakly bound water. The large isotropic shifts of the 27−84 ppm resonances are ascribed to the Fermi-contact

(58) Barrero, C. A.; Garcia, K. E.; Morales, A. L.; Kodjikian, S.; Greneche, J. M. *J. Phys.: Condens. Matter* **2006**, *18*, 6827.

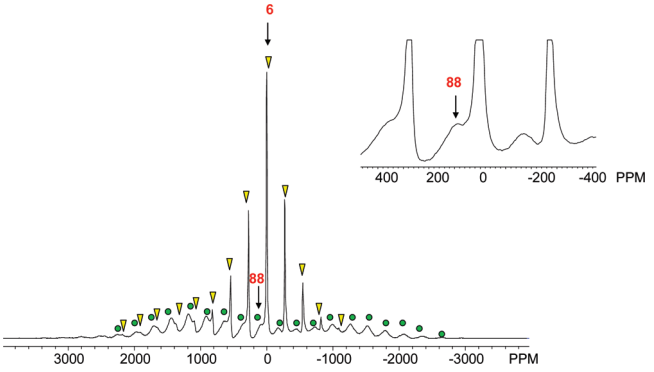

Figure 6. ^{2}H MAS NMR spectrum of β-FeOOH (Aka-n) acquired at room temperature (15 kHz spinning speed).

shift (hyperfine shift) interaction which arises from the through-bond transfer of spin-density from the unpaired electrons of the Fe^{3+} ions to the nucleus under observation (^{2}H).[50,59,60] The magnitude of hyperfine shift depends on both the local structure and the molar magnetic susceptibility, χ_M; as explained in previous work, a reduced value of χ_M, due to residual antiferromagnetic correlations, leads to a smaller shift.[30] The isotropic peak at 84 ppm is assigned to Fe_3OH H^+ sites inside the tunnels (Figure 1). When the structure of akaganeite is cleaved along the (100) or (001) plane, the Fe_3OH sites originally inside the tunnel are exposed and now become surface sites (Figure 1). Thus the signal at 84 ppm should also contain a contribution from these surface sites. The Fe_3OH local environments are similar to the proton environments found in goethite. These sites gave rise to a resonance at 90 ppm in micrometer-sized goethite, micrometer-sized goethite having a similar χ_M value of 24×10^{-6} emu/(g Oe)[28,61] to that of akaganeite ($\chi_M = 30 \times 10^{-6}$ emu/(g Oe)),[62] confirming our assignment. The resonance at 27 ppm is tentatively assigned to the extra proton site in the pocket inside the tunnel (Figure 1),[34] on the basis of its weaker intensity and smaller shift (the occupancy of the extra proton site is low and it is more weakly bound to the akaganeite framework). However, the relative intensity of the 27 ppm peak to the 84 ppm peak is higher than expected on the basis of the Cl^- content determined by elemental analysis. This may be due to a longer spin−spin/spin−lattice (T_2/T_1) relaxation time of the signal from the extra proton, because of its smaller hyperfine shift. It is also possible that part of this broad, overlapping resonance arises from water molecules inside the tunnels.

No shift in the ^{2}H isotropic resonances of Aka-m was observed on heating this sample up to 120 °C (Figure 4). This is not consistent with the $1/T$ dependence of the shift expected for a system obeying the Curie−Weiss law. However, the result is not surprising since there is no significant change in the magnetic susceptibility (χ) of akaganeite in this experimental temperature range, due to the existence of significant residual antiferromagnetic couplings between Fe^{3+} ions at these temperatures.[1,8,63,64] The 4.8 ppm resonance sharpened noticeably on heating, and increased in intensity. This most likely arises because water molecules are released from the tunnels, which are then bound weakly to the akaganeite surfaces. The water molecules remain mobile on returning to room temperature, as seen by the sharp 4.8 ppm resonance, and associated narrow spinning sideband manifold; the change in line width of this resonance confirms that a redistribution of the water locations has occurred. The sidebands of 27 ppm resonance sharpen on heating (see Figure 4 and Figure S4 in the Supporting Information), suggesting that the tunnel species associated with this resonance become more mobile.

Even though Aka-m contains a significant amount of water, a distinct resonance due to the water in the tunnels was not observed. As discussed above, the water resonance may be buried under the 27 ppm resonance, but even then, the intensity of the 27 ppm resonance is too weak to account for the missing water. Slow motional modes of the water (with correlation times, $\tau_c \approx 20-200$ μs), which interfere with the ability of MAS to refocus the ^{2}H signal, may account for the lack of signal. We have observed this phenomenon for many hydrated and deuterated solids, including electrolytic manganese dioxide.[59,65] To test this hypothesis, we obtained lower temperature spectra from Aka-m (Figure 5). On cooling to 0 °C, i.e., just below T_N, a noticeable increase in relative intensity of the resonance at approximately 4.8 ppm was observed, supporting the proposal that some of the water signal may be lost due to motional processes. The FeO_3H resonance broadens considerably below T_N, and unfortunately, the ^{2}H NMR spectrum at −50 °C showed a featureless resonance with an extremely poor signal-to-noise (S/N) ratio. Hence it was not possible to explore the water dynamics over a larger temperature range. The broadening of the signal, to the point where it is barely visible above the noise, is ascribed to the large fluctuating fields that are seen by the ^{2}H nuclei, even in the antiferromagnetic state (close to T_N). A similar phenomenon was previously observed in our study of goethite.[28] No significant modification of the local environments was observed in the NMR spectra after cooling and reheating.

When the particle size of akaganeite was reduced to about 5 nm, the relative intensity of the ^{2}H 27 ppm resonance decreased and the resonance could no longer be resolved (Figure 6). This is ascribed to (i) the smaller number of extra protons in the tunnel, because of the higher pH used in the synthesis of Aka-n (pH 3.4) in comparison to that used for Aka-m (pH 1.5), and (ii) the severe overlap of the 27 ppm resonance with the much more intense 6 ppm surface water resonance. The increased intensity of the 6 ppm resonance was ascribed to the much higher surface area of the Aka-n sample.

(59) Paik, Y.; Osegovic, J. P.; Wang, F.; Bowden, W.; Grey, C. P. *J. Am. Chem. Soc.* **2001**, *123*, 9367.
(60) Nayeem, A.; Yesinowski, J. P. *J. Chem. Phys.* **1988**, *89*, 4600.
(61) Ozdemir, O.; Dunlop, D. J. *Geophys. Res. Lett.* **1996**, *23*, 921.
(62) Kulgawczuk, D. S.; Obuszko, Z.; Szytuza, A. *Phys. Status Solidi* **1968**, *26*, K83.
(63) Chambaere, D.; Grave, E. D. *J. Magn. Magn. Mater* **1983**, *42*, 263.
(64) Fan, H.; Song, B.; Yang, Z.; Li, Q. *Chem. Lett.* **2004**, *33*, 576.
(65) Paik, Y.; Bowden, W.; Richards, T.; Grey, C. P. *J. Electrochem. Soc.* **2005**, *152*, A1539.

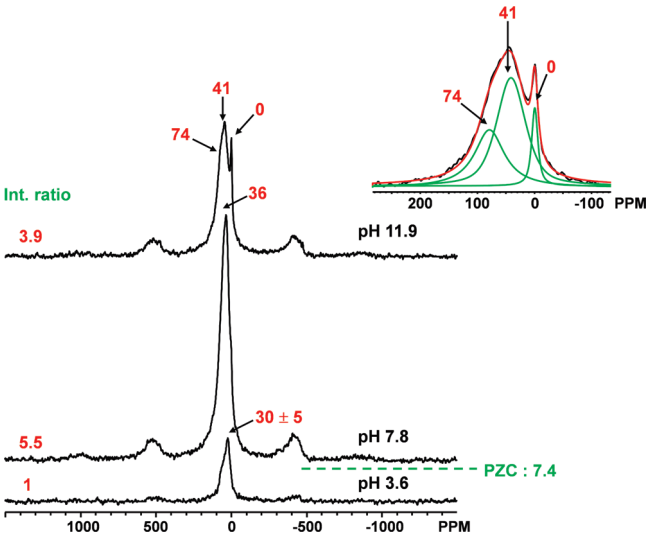

Figure 7. ^{7}Li MAS NMR spectra of Li^{+}-sorbed micrometer-sized akaganeite (Aka-m-3.6, 7.8, and 11.9) as a function of pH, collected at a spinning rate of 37 kHz. The resonances are labeled with their isotropic shift positions. The integrated intensities of the higher frequency (30−74 ppm) resonances (normalized to the intensity of the resonance of the pH 3.6 sample) and the pH of the solutions are shown on the left and right-hand sides, respectively. Right upper corner inset: Deconvolution of Aka-m-11.9 spectrum (green peaks and red lines (sum)).

3.2.2. ^{7}Li NMR of Li-Sorbed Aka-m and Aka-n As a Function of pH. Two ^{7}Li resonances at about 0 and 30−36 ppm (major) were observed at low and neutral pH, the intensity of the peak at about 30−36 ppm increasing by a factor of 5.5 as the pH increased from pH 3.6 to 7.8, i.e., to above the PZC value of akaganeite (Figure 7). The low intensity of the Aka-m-3.6 resonances is ascribed to the positively charged FeOOH surfaces at this pH. When the pH was adjusted to 11.9, two new resonances at 41 and 74 ppm, with relative intensities of 1.8:1 were observed. The intensities of these resonances were approximately 30% weaker, compared to that of the 36 ppm resonance at neutral pH, indicating a different strength and mode of binding. Unlike Aka-m, a pronounced increase in intensity of the 77 ppm resonance was observed on going from pH 8.2 to 11.3 for Aka-n samples (Figure 8), along with the appearance of a new resonance at 138 ppm.

The peaks at 30−36, 41, 74, and 138 ppm are assigned to Li ions in inner-sphere complexes having direct Li−O−Fe interactions with the surface of akaganeite; these large shifts, as in the ^{2}H spectra, arise from the Fermi-contact shift mechanism which involves direct transfer of spin density through the (Li−O−Fe) bonds.[30] Adsorption densities for Aka-m-7.8 and -11.9 were calculated by using the total ^{7}Li signal intensity of the inner sphere resonances and the Aka-m BET surface area of 33 m^2/g giving high densities of 0.6×0.6 nm^2/Li^+ (2.7 Li^+/nm^2) and 0.72×0.72 nm^2/Li^+ (1.9 Li^+/nm^2), respectively. This analysis took into account the 24% signal loss due to T_2 relaxation during two rotor periods (39 μs) of the spin−echo pulse sequence. (The T_2 values for the Aka-m-11.9 resonances were approximately 0.14 ms; the T_2 values for the major resonances of Aka-m-7.8 were assumed to be similar). The decrease of the adsorption density from pH 7.8 to 11.9 is ascribed to the formation of a $LiFeO_2$ precipitate

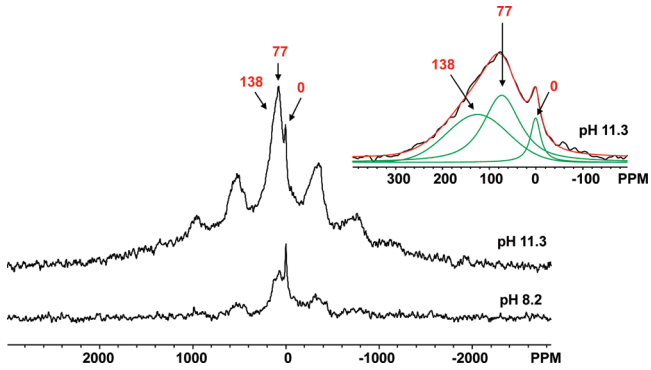

Figure 8. ^{7}Li MAS NMR spectra of Li^{+}-sorbed nanoakaganeite (Aka-n-8.2 and Aka-n-11.3) as a function of pH, collected at a spinning rate of 34 kHz. pH values of the solutions are shown on the right-hand side. Right inset: Deconvolution of Aka-n-11.3 spectrum (green peaks and red lines (sum)).

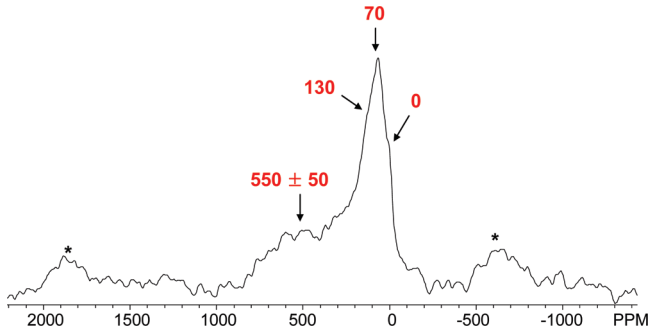

Figure 9. ^{6}Li MAS NMR spectrum of ^{6}Li-sorbed Aka-m at a spinning speed of 37 kHz. The isotropic resonances are labeled (* indicates spinning sidebands in this and the next plot).

at very high pH. To test this hypothesis, we prepared a ^{6}Li-sorbed sample in the same manner as Aka-m-11.9, but we used a longer sorption equilibrium time. A very broad 550 ppm peak (with an intensity ratio of 1.5 for the 550:(70 + 130 ppm) resonances) was now observed in the ^{6}Li NMR experiment, the large shift being typical for a Li local environment in an α-$LiFeO_2$ phase[66] (Figure 9). This confirms that some dissolution and reprecipitation of Fe^{3+} occurs forming a lithium iron oxide. The formation of a significant amount of precipitate at this high pH is not surprising, as akaganeite is the least stable iron oxyhydroxide.

The 0 ppm resonances were assigned to outer-sphere complexes because of their small shift. Moderately short T_1 times ($\approx$ 0.1 s) were observed for these species, which are noticeably shorter than those typically found for diamagnetic Li-containing compounds (>60 s), again suggesting that these are surface species and not impurities. This assignment is consistent with our recent work on lepidocrocite (γ-FeOOH) where the intensity of the 0 ppm peak was monitored as a function of relative humidity.[30] In the akaganeite systems, the 0 ppm peak intensities increased as a function of pH, though the changes are less significant than seen for the hyperfine shifted peaks (Figures 7 and 8). The increase in outer-sphere complex formation is attributed to the increase in concentration of

(66) Pan, C. Li NMR Studies of $LiMO_2$. M.Sc. Thesis, SUNY Stony Brook, NY, 2000.

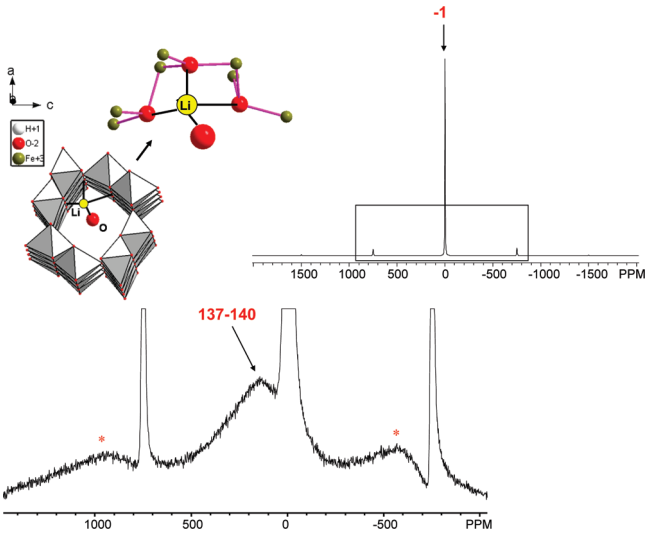

Figure 10. Zoom of the ^{7}Li MAS NMR spectrum of tunnel-structured $LiFeO_2$ acquired at a spinning speed of 58 kHz. Upper right corner inset: full spectrum; black rectangular box indicates the zoomed region. Upper left corner inset: Li^+ ions in the vacant tetrahedral sites inside the $LiFeO_2$ tunnels. The protons in the structure have been removed for clarity.

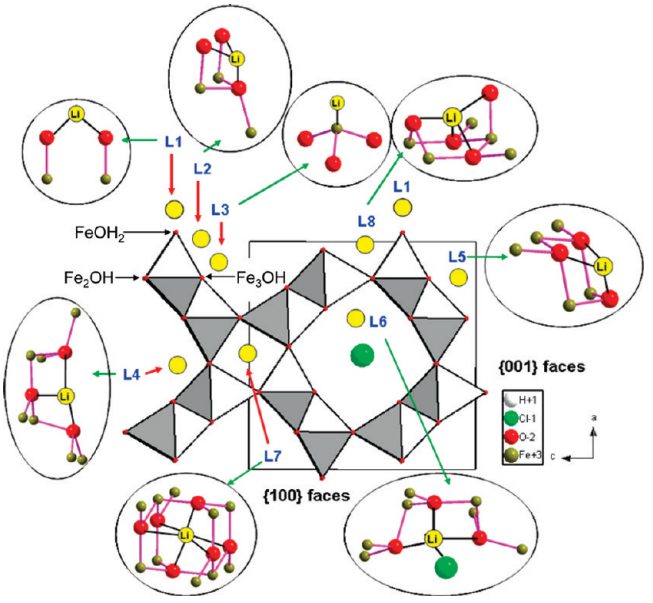

Figure 11. Possible positions for the lithium cations on the surface of akaganeite. The proton atoms in the structure and coordinated to the surface bound oxygen anions have been removed for clarity. $FeOH_2$, Fe_2OH, and Fe_3OH sites are labeled.

weak negative charges, the various surface oxygen ions on the surface of akaganeite becoming increasingly deprotonated as pH increases.[67]

3.2.3. ^{7}Li NMR of Tunnel-Structured $LiFeO_2$ and Identification of the Li^+ Positions on the Akaganeite Surface. To aid in the assignments of the various ^{7}Li resonances, we acquired a ^{7}Li NMR spectrum of the $LiFeO_2$ tunnel structure, observing a very broad resonance of 137 ± 3 ppm (Figure 10). The Li^+ ions in this tunnel structure are bound to three framework O sites, each O atom being bound to 3 Fe^{3+} ions (Figure 10).[6] Because the size of the Fermi-contact shift depends strongly on the number of Li−O−Fe bonds, we adopt the same approach adopted in our earlier paper[30] and estimate an average contribution per Li−O−Fe(III) connectivity to the overall hyperfine shift of 15 ppm (i.e., 137/9 ppm). This value is of the same order of magnitude, but smaller, than the values observed for Li−O−Fe(III) connectivities in goethite and lepidocrocite of 24 and 20 ppm, respectively.[29,30] The values for goethite and lepidocrocite were similarly obtained by an analysis of the ^{6,7}Li shifts and number of Li−O−Fe(III) connectivities in Li^+-exchanged goethite and lepidocrocite. These variations cannot be explained by changes in the bulk magnetic susceptibility, since the values for goethite ($\chi_M = 24 \times 10^{-6}$ emu/(g Oe)) are slightly slower than those of akaganeite ($\chi_M = 30 \times 10^{-6}$ emu/(g Oe)), and noticeably lower than lepidocrocite ($\chi_M = 110 \times 10^{-6}$ emu/(g Oe)).[28,61,62] Furthermore, the ^{2}H shifts for the Fe_3OD groups in goethite and lepidocrocite are similar. Differences in Li−O−Fe bond angles, bond lengths, and Li^+ coordination numbers (octahedral vs tetrahedral) must also be responsible for these variations, as found for many other systems, and seen in recent density functional theory calculations.[47,68−70] To explore the errors that may be caused by assuming that every Li−O−Fe(III) connectivity contributes equally to the total hyperfine shift, we will, in the subsequent analysis, also consider the effect of utilizing the value for the Li−O−Fe(III) shift obtained for goethite. This appears reasonable, because the ^{2}H shifts and χ_M are similar for this system.

Using the shift estimated per Li−O−Fe(III) connectivity for akaganeite (i.e., 15 ppm), the 30−36 ppm resonances seen at low and neutral pH and the 41 ppm peaks seen at high pH can be assigned to Li^+ ions that are either coordinated to two oxygen atoms that are each bound to only one Fe^{3+} ion (i.e., 2 Li−O−Fe^{3+} linkages) or to only one oxygen atom that is bound to two Fe^{3+} ions (i.e., 1 Li−O(−Fe^{3+})$_2$ link). The peak shift from 30 to 36 to 41 ppm is ascribed to stronger Li^+−O^{2-} binding at high pH or to the formation of a third Li−O−Fe linkage. Similarly, the resonances at 75 and 138 ppm are due to 5 and 9 Li−O−Fe interactions, respectively. We will now explore the modes of Li^+ surface binding that are commensurate with these numbers of Li−O−Fe(III) connectivities.

The akaganeite surface is dominated by two faces, (100) and (001).[1] We assume that these faces represent the main adsorption planes on the surface, an assumption that is consistent with the high sorption sites for Li in this system. In acidic conditions, these faces are terminated via two reactive groups, Fe_3OH and $FeOH_2$, and one inert Fe_2OH group (Figures 1 and 11), the latter being difficult to deprotonate.[67] Plausible surface adsorption sites on the surface at each pH condition can then be proposed (Figure 11), and categorized, on the basis of their number of Li−O−Fe interactions (Table 1).

(67) Venema, P.; Hiemstra, T.; Weidler, P. G.; van Riemsdijk, W. H. *J. Colloid Interface Sci.* **1998**, *198*, 282.
(68) Lee, Y. J.; Eng, C.; Grey, C. P. *J. Electrochem. Soc.* **2001**, *148*, A249.
(69) Lee, Y. J.; Grey, C. P. *Chem. Mater.* **2000**, *12*, 3871.
(70) Lee, Y. J.; Park, S.-H.; Eng, C.; Parise, J. B.; Grey, C. P. *Chem. Mater.* **2001**, *14*, 194.

Table 1. Estimated Hyperfine Shifts for Possible Li^+ Adsorption Sites (shown in Figure 11, Calculated by Using the Average Shift Value Estimated for Each Akaganeite Li−O−Fe(III) Interaction and the Number of Li−O−Fe Bonds[a]

sites	no. of Li−O−Fe bonds	NMR shift (ppm)
L1	2	30 (48)
L2	5	75 (120)
L3	3	45 (72)
L4	9	135 (216)
L5	8	120 (192)
L6	9	135 (216)
L7	18	270 (432)
L8	9	≤135 (216)

[a] NMR shifts given in parentheses represent those estimated by using the average shift value found for Li−O−Fe(III) interactions in goethite.[29].

Only one site can be readily identified that has only two Li−O−Fe interactions (the L1 site). This binuclear bidentate site is formed by Li^+ binding to the oxygen ions of two terminal FeOH groups (Figures 1 and 11). The availability of these oxygen ions for binding is consistent with the basicities of the different sites, the $FeOH_2$ groups being deprotonated at lower pH than the Fe_3OH groups.[67] Thus there will likely be a higher concentration of negatively charged FeOH oxygen atoms than Fe_3O oxygen ions at moderate-to-low pH values. We therefore assign the resonances at 30−36 ppm and 41 ppm, observed under acidic and neutral conditions, to this L1 binuclear bidentate site. The error associated with the shift value associated with each Li−O−Fe(III) interaction does not alter this assignment: use of the goethite values leads only to the suggestion that one Li−O bond in the binuclear complex may be weaker, and that the complex may be asymmetric. Given that the terminal Fe−O group is still protonated, the formation of a linear Fe−O−Li^+ binding arrangement appears unlikely, and the prediction that a bent Fe−O(H)−Li^+ configuration is formed, which can then bind to the adjacent FeO(H) oxygen ion appears reasonable.

The L3 site (Figure 11) consists of a Li^+ ion bound to a Fe_3O oxygen ion. This site will therefore be associated with three Li−O−Fe(III) connectivies, and will also have small shift (45 ppm, Table 1). The Fe_3OH proton is less acidic relative to the second $FeOH_2$ proton and should only be deprotonated in very basic conditions (e.g., pH 11.9). Thus this binding site should increasingly contribute to the intensity of the Li signal, as the pH is increased, accounting for the shift of the major ^{7}Li resonance from 30 to 41 ppm.

At high pH, the Li^+ ions can also bind to both FeOH and Fe_3O oxygen atoms, giving rise to the L2 site. The ^{7}Li resonance seen at high pH values at 74−77 ppm is assigned to this environment, based on the Li−O−Fe(III) akaganeite shift values. Use of the goethite Li−O−Fe(III) leads to a different assignment, namely, that the 74−77 ppm resonance is simply due to the L3 site. However, the use of either Li−O−Fe(III) shift value leads to the same conclusion, namely, the Fe_3O environment is involved at high pH, the two structural models simply differing in the extent to which the Li^+ binds to the nearby FeOH oxygen atoms.

The 138 ppm peak of Aka-n-11.3 can be assigned to L6 and L4 sites, both sites having 9 Li−O−Fe interactions. The nanosized particles are expected to have an increased number of easily accessible L6 tunnel sites to adsorb Li^+ ions, because of the smaller aspect ratios of these particles, as compared to micrometer-sized particles. Thus, given that the 138 ppm resonance predominates in the Aka-n and not Aka-m samples, it is likely that the major contribution for this site arises from the L6 sites in the tunnels. The L5 and L7 sites were ruled out, because the estimated hyperfine shifts of these sites do not match with any observed shifts (Table 1). In addition, the L5 and L8 sites are not predicted to form strong binding with Li^+ because of the involvement of the inert Fe_2OH sites (Figure 1 and 11). Again, use of the goethite Li−O−Fe(III) shift values suggests that sites such as the L2 site may also contribute to the 138 ppm signal. However, we note that since the L4 and L6 sites have local environments that are essentially identical to those found in the ion-exchanged akaganeite sample, it is likely that the Li−O−Fe(III) akaganeite, and not goethite, shift values should lead to the more accurate predictions for the overall hyperfine shift for these sites. Variable-temperature ^{7}Li MAS NMR of Aka-m-11.9 is in agreement with these assignments, showing an increase in the 130 ppm resonance at the highest temperature studied (125 °C), at the expense of a weak peak at approximately 27 ppm (assigned to L1), the loss of water presumably from both the surface and tunnels favoring the occupancy of sites where the Li^+ is bound to more surface oxygen sites (see Figure S5 in the Supporting Information).

Because this work completes our study of the three different FeO(OH) polymorphs,[29,30] comparisons between cation binding to these three related but structurally distinct polymorphs can now be made, allowing the generality between Li^+ binding motifs to be explored. At low pH, binuclear, bidentate binding modes to the FeOH groups were also observed for both lepidocrocite and goethite. For goethite, binding to the Fe_3O oxygen also becomes possible at higher pH, resulting in a larger number of Li−O−Fe connectivities. The significantly increased loading level of Li^+ on the surface of akaganeite (Aka-m) (1.9−2.7 Li^+/nm^2 above its PZC) by a factor of about 20 as compared to that of lepidocrocite (0.1 Li^+/nm^2),[30] is consistent with our assertion that the dominant surfaces (i.e., the (100) and (001) faces) of akaganeite represent the major adsorption planes. Binding sites in lepidocrocite, by contrast, were located on the minor surfaces. The results indicate that akaganeite is a better system for the adsorption of small cations than lepidocrocite, because it has more $FeOH_2$ and Fe_3OH sites, along with additional sites at the entrances to the tunnel. Binding to akaganeite is similar to that found for goethite, except that the stability of akaganeite may be an issue at higher pH. Finally, we note that the availability of data for all three systems allows the errors associated with our method for assigning resonances to specific environments based on average Li−O−Fe(III) shifts to be explored. For example, we were able to use the NMR data available

for both goethite and akaganeite, to compare the surface sites predicted with the two (goethite and akaganeite) different average Li−O−Fe(III) values. Clearly, the next step in the analysis is to (a) account for different Li−O−Fe bond angles and distances, and (b) explore the effect of variations in the residual magnetic couplings between the surface and the bulk. Both effects are currently being explored by performing DFT calculations.

4. Summary and Conclusions

The hydroxyl groups of the paramagnetic iron oxyhydroxide polymorph akaganeite were characterized by using ^{2}H MAS NMR spectroscopy, showing the existence of the rigid OH groups within the FeO_6 tunnels. Lithium binding sites were also quantified and characterized by using ^{7}Li MAS NMR spectroscopy and inner-sphere and outer-sphere complexes were clearly separated, on the basis of the observed large hyperfine shifts for the inner sphere complexes. Several possible adsorption sites of Li^+ were suggested on the basis of the sizes of the hyperfine shift. At around neutral pH, Li^+ forms a bidentate complex on the (001) or (100) face of akaganeite, involving terminal FeOH groups (i.e., O_5Fe-OH octahedra). At high pH, Fe_3OH oxygen sites on the faces become deprotonated, resulting in the formation of monodentate and multidentate complexes involving both oxygen atoms of Fe_3O and FeOH groups. Li binding to sites at the entrances of the tunnels are also observed for samples with the smallest aspect ratios.

The present results, in combination with our previous results for the other FeO(OH) polymorphs, suggest general trends for binding, which are likely to be applicable to the binding of cations to other hydroxylated surfaces. At lower pH values, where fewer of the surface sites are deprotonated, binding configurations to fewer oxygen anions occur (two, in the case of iron oxyhydroxides). As the pH increases, the surfaces are deprotonated further; binding motifs involving more surface oxygen anions will be seen, if the surfaces contain steps or pockets (formed by the tunnels, in this case) that will allow for multidentate binding. Furthermore, as the more basic sites are deprotonated, sites become available for cation binding that can form stronger adsorption complexes. Binding to these sites may compete with sites involving binding to multiple surface oxygen sites, even though the binding may occur via the formation of fewer metal(M)−O bonds (or interactions) with the surface oxygen anions, because the individual M−O interactions may be stronger. The relative importance of the different binding motifs will depend on the concentrations of the different environments, the strength of the different M−O interactions, and the extent of surface hydration: As the surface is dried and the Li^+ ions lose their waters of hydration, Li^+ binding to the surface involving greater numbers of $Li^+-O_{(surface)}$ should become more favorable. Clearly, the difference in the strengths of binding of different cations to various surfaces lie in specific surface structures, but we show that NMR spectroscopy can, at least in some circumstances, help to unravel the various factors.

In conclusion, via this contribution, we clearly demonstrate that MAS NMR spectroscopy is a useful technique with which to study ion binding on poorly characterized systems such as disordered materials, nanoparticles, or systems where large single crystals are not available. Similar NMR approaches can be applied to the study of ion binding modes at water−solid interfaces in other magnetically challenging paramagnetic systems such as those found in alkaline batteries or some water splitting catalysts.

Acknowledgment. This work was funded by NSF grants (CHE-0021934; Center for Environmental Molecular Science (CEMS) and the Collaborative research grant in chemistry, CRC-1065905). We acknowledge James Kubicki and Ulla Gro Nielsen for helpful discussions.

Supporting Information Available: XRD patterns for Aka-m, Aka-m-3.6, Aka-m-7.8, and Aka-m-11.9; PZC for Aka-m; TGA data for Aka-m, Aka-m-11.9, and Aka-n; enlargement of part of Figure 4 (PDF). This material is available free of charge via the Internet at http://pubs.acs.org.